Comments on "Accuracy of Raman lidar water vapor calibration and its applicability to long-term measurements"

David N. Whiteman,[1,*] Demetrius Venable,[2] and Eduardo Landulfo[3]

[1]Laboratory for Atmospheres, National Aeronautics and Space Administration/Goddard Space Flight Center, Greenbelt, Maryland 20771, USA

[2]Physics and Astronomy Department, Howard University, Washington, DC, USA

[3]Centro de Lasers e Aplicações, Instituto de Pesquisas Energéticas e Nucleares, Sãu Paolo, Brazil

*Corresponding author: david.n.whiteman@nasa.gov

Received 7 June 2010; accepted 11 July 2010;
posted 25 March 2011 (Doc. ID 129548); published 13 May 2011

In a recent publication, Leblanc and McDermid [Appl. Opt., **47**, 5592 (2008)] proposed a hybrid calibration technique for Raman water vapor lidar involving a tungsten lamp and radiosondes. Measurements made with the lidar telescope viewing the calibration lamp were used to stabilize the lidar calibration determined by comparison with radiosonde. The technique provided a significantly more stable calibration constant than radiosondes used alone. The technique involves the use of a calibration lamp in a fixed position in front of the lidar receiver aperture. We examine this configuration and find that such a configuration likely does not properly sample the full lidar system optical efficiency. While the technique is a useful addition to the use of radiosondes alone for lidar calibration, it is important to understand the scenarios under which it will not provide an accurate quantification of system optical efficiency changes. We offer examples of these scenarios. Scanning of the full telescope aperture with the calibration lamp can circumvent most of these limitations. Based on the work done to date, it seems likely that the use of multiple calibration lamps in different fixed positions in front of the telescope may provide sufficient redundancy for long-term calibration needs. Further full-aperture scanning experiments, performed over an extended period of time, are needed to determine a "best practice" for the use of multiple calibration lamps in the hybrid technique.

OCIS codes: 120.0120, 280.0280.

1. Introduction

The Network for the Detection of Atmospheric Composition Change (NDACC) has recently established long-term monitoring of water vapor using Raman lidar as one of its core objectives [1]. Other international efforts such as the Global Climate Observing System Reference Upper Air Network [2] are tasked with the same objective. One of the paramount needs for developing a long-term dataset for monitoring atmospheric trends is a calibration that varies randomly around some mean value and does not involve step jumps of unknown magnitude [3] or significant drifts. These calibration changes increase the time required to detect atmospheric trends, which is already typically measured in decades [4,5]. For this reason, it is important to carefully examine any calibration techniques developed for ensuring stable, long-term calibrations. Here we examine the hybrid lamp technique proposed by [6] for calibration of Raman water vapor lidar.

0003-6935/11/152170-07$15.00/0

2. Calculation of Water Vapor Mixing Ratio from Raman Lidar

The water vapor mixing ratio can be expressed as [7,8]

$$w = k\frac{O_N(r)}{O_H(r)}\frac{F_N(T)}{F_H(T)}\frac{P(\lambda_H,r)}{P(\lambda_N,r)}\frac{\frac{d\sigma_N(\pi)}{d\Omega}}{\frac{d\sigma_H(\pi)}{d\Omega}}\frac{\xi(\lambda_N)}{\xi(\lambda_H)}\Delta\tau(\lambda_N,\lambda_H,r), \tag{1}$$

where k is a factor determined by molecular weights and volume mixing ratios and is ≈0.485. $O_X(r)$ represents the channel overlap function as a function of range, r for channel X, which in this case, would be either the nitrogen, N, or water vapor channel, H. $F_X(T)$ is a temperature dependent factor that accounts for the temperature dependence of Raman scattering. $P(\lambda_X,r)$ is the backscattered power (after subtracting any background contribution due, for example, to skylight or detector noise). $\xi(\lambda_X)$ represents the total lidar receiver optical efficiency, ξ, at the laser wavelength, λ_X, and includes factors such as the reflectivity of the telescope, the transmission of any conditioning or wavelength selection optics, the transmission of any filters, and the quantum efficiency of the detector. $\frac{d\sigma_X(\pi)}{d\Omega}$ represents the differential Raman backscattering cross section, and $\Delta\tau(\lambda_N,\lambda_H,r)$ represents the atmospheric differential transmission at the water vapor and nitrogen wavelengths.

The term of interest in Eq. (1) is the efficiency ratio, $\frac{\xi(\lambda_N)}{\xi(\lambda_H)}$, which includes the transmission or reflection efficiency of all optical components, and given that reflection and transmission efficiencies can change as a function of position on each optical component, it is a weighted average of the portions of these components in use. We will first consider the use of a calibration lamp in a fixed position in front of the telescope and then discuss the influence of position-dependent efficiency changes.

3. Use of a Calibration Lamp in a Fixed Position

The technique proposed in [6] involves a tungsten calibration lamp powered by a stabilized current source. The use of a calibration lamp is very attractive as a component of a Raman water vapor lidar calibration technique, since the quantity that must be evaluated with accuracy is the ratio of the transmission efficiencies at the Raman water vapor (407.5 nm) and nitrogen (386.7 nm) wavelengths, and the ratio of the intensities of these lamps at the desired wavelengths is very stable.

A. Stability of the Lamp Intensity Ratio

An examination of 200 W calibration lamps obtained over a period of several years indicated that the effective color temperature of these lamps varied typically within a range of ±10–20 K [9]. This color temperature range implies different spectral outputs for the lamps, which for the small spectral range of 386.7–407.5 nm, can be approximated with high accuracy by the Planck black body formula. Evaluating the Planck formula at 386.7 and 407.5 nm for changes in lamp color temperatures of ±20 K indicates that the ratio of spectral outputs at these two wavelengths varies by 0.3% or less. This implies that the use of uncalibrated tungsten lamps likely supplies a spectral reference for the ratio of water vapor and nitrogen channel optical efficiencies that is accurate to better than 0.3%. The use of a tungsten lamp with calibration traceable to National Institute of Standards and Technology standards to within 2% reduces the uncertainty in this ratio to ~0.1%. Therefore, the calibration lamps provide a highly stable reference for use in a Raman water vapor lidar calibration. But the primary question to be addressed here is whether the full lidar system efficiency is well represented by using a lamp at a fixed position in front of the lidar receiver.

B. Ray Trace of a Calibration Lamp

Figure 1 shows the ray trace of a calibration lamp placed in front of a telescope and receiver system. The lamp is positioned near the edge of the primary aperture and emits in all directions. By virtue of a field stop used at the prime focus of the telescope, only those rays that diverge from the optical axis within an angle of ± one-half the angular field of view will be accepted by the field stop. The right of Fig 1 shows the pattern of rays that will be transmitted fully through the optical train of the lidar system due to this angular filtering.

This figure illustrates the concern of using a lamp at a fixed position in front of the telescope aperture. Only a very small fraction of the telescope primary mirror and all optics that follow it in the optical train are sampled by the direct beam from the lamp.

C. Reflections from Uncalibrated Surfaces

Leblanc and McDermid [6] discuss performing their lamp calibration measurements with the hatch that protects the lidar system closed. The light from the lamp is able to reflect off of the hatch cover and thus illuminate the entire telescope. The use of this technique raises some questions, however. What is the spectral response of the hatch cover and how stable is this response (e.g., is the hatch kept clean)? One can observe from Fig. 8 of [6] that closing the hatch changes the measured ratio by about 15%. This implies that the reflectivities of the hatch at 407.5 and 386.7 nm are not the same. So the spectral characteristics of the light that is reflected off of the hatch is significantly different than the calibrated light that enters the telescope directly from the lamp.

Another question is: what fraction of the entire signal sampled by the telescope is due to the direct beam versus the signal that is reflected off of other surfaces? In an attempt to address this question, an experimental configuration similar to that illustrated in Fig. 5 from [6] was established using the Howard University Raman Lidar (HURL) in Beltsville, Maryland. The calibration lamp was

placed approximately 1 m away from the telescope, and a white reflective board was placed approximately 30 cm above the lamp. An examination of the signal intensity with and without this reflective board in place indicated that approximately 90% of the signal was due to the direct beam and only 10% from the reflected beam. These results indicate that even the use of a reflective hatch can yield a telescope illumination that is strongly biased by the efficiency characteristics of the small fraction of the optical train illuminated by the forward beam as illustrated in Fig. 1. The use of a reflective hatch may not evenly fill the telescope aperture, and the component of the lamp output that is reflected from other surfaces will likely not retain the spectral characteristics of the lamp. Therefore, it seems best to avoid reflections from uncalibrated surfaces in performing lamp-based lidar calibrations.

D. Consideration of Fiber Optics

The uneven illumination of the telescope shown in Fig. 1, as apparent from the results of the experiment just described, propagates through the entire optical train to the detectors. If there are position-dependent optical efficiencies in any of the optical components, the small fraction of the telescope sampled by the lamp may not properly represent the efficiency of the entire optical train. This statement pertains to a bulk optics configuration where the signal focussed by the telescope is collimated using traditional optics. Does the use of an optical fiber at the prime focus of the telescope improve this situation? Even with an optical fiber at the prime focus of the telescope, the experiment just described indicates that the efficiency of the telescope primary and secondary (if used) will be heavily weighted by the small spot illuminated by the lamp's forward beam. This effect is not changed by the use of a fiber. But does a fiber help to scramble the signal for the rest of the optical train removing concern about position-dependent efficiency changes elsewhere in the optical train?

To investigate this, an experiment was performed again on the HURL with the reflective board mentioned above in place. A calibration lamp was moved along a line from one edge of the telescope receiver to the other, and the pattern emitted by an optical fiber placed at the prime focus of the telescope was recorded by training the light from the fiber on a screen and photographing the screen. Fig. 2 shows the results of this experiment.

There are several things to note in Fig. 2. First, the output of the fiber shows one or a set of modes being excited in the multimode fiber by the calibration lamp. As the position of the lamp changes, the mode pattern changes as well. The optical information from a small portion of the telescope is converted into a ring of varying diameter depending on the fiber modes in use. This is just a single experiment on a particular multimode fiber, but it indicates that fiber optics do not in general scramble the optical signal sufficiently to remove concern about the position dependence of efficiences in the optical train.

4. Position Dependence of Optical Efficiencies in the Lidar Optical System

The preceding discussion strives to make the point that a calibration technique based on the use of a calibration lamp in a fixed position in front of a telescope will not equally sample the telescope or receiver optics. In the experiment described above, even with a reflective surface above the telescope, the signal arriving at the prime focus of the telescope was dominated by the forward beam from the lamp. If the optical efficiency of some section of the primary

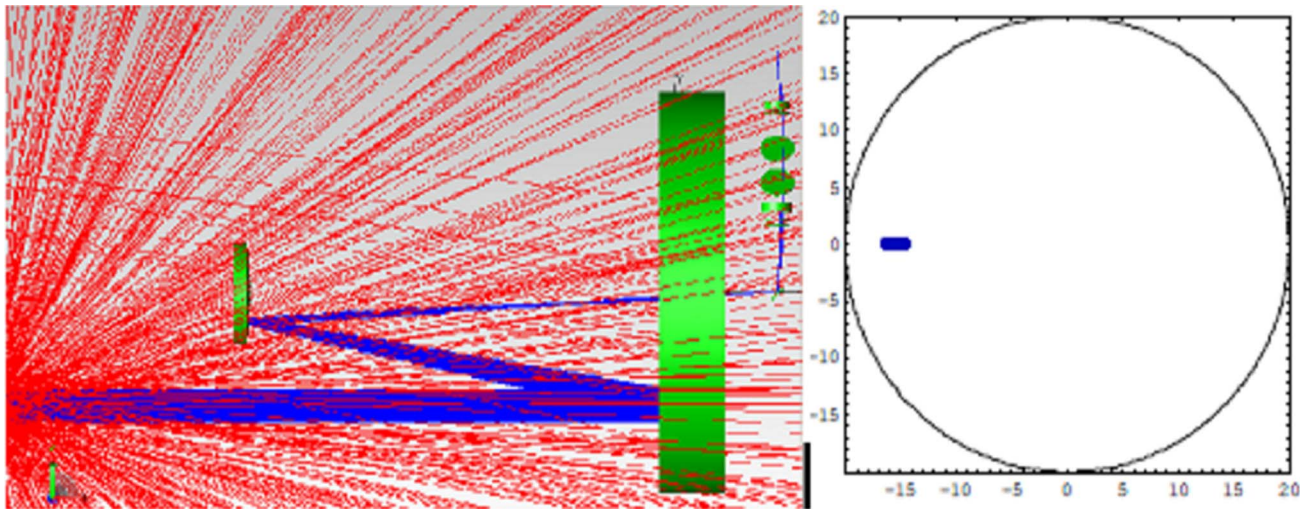

Fig. 1. (Color online) Ray trace of a spectral lamp at a fixed position in front of a telescope system. The Cassegrain telescope consists of a primary and secondary. Also, beam handling optics are shown behind the telescope primary. The red rays indicate the lamp output in all directions. The blue rays are those that fall within the angular field of view of the telescope system and are thus permitted to propagate down the lidar optical train. (Right) The large circle indicates the size of the collimated light bundle created by the beam handling optics shown. The blue rays are those that are permitted to pass through the optical system. These are the rays that fall within +/ – fov/2 of a line parallel to the optical axis.

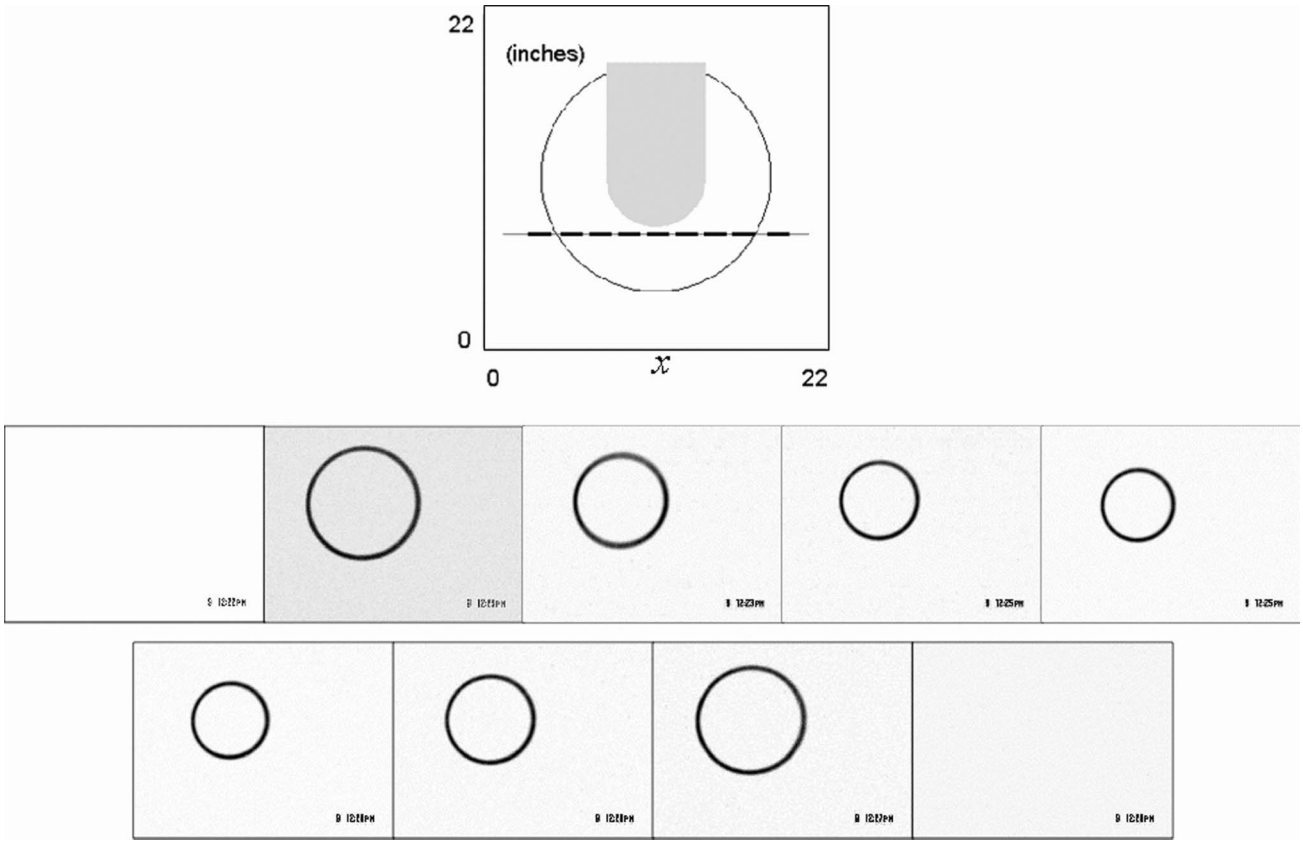

Fig. 2. Tungsten lamp is placed at varying positions in front of the HURL telescope as shown in the diagram at the top of the figure. The output from a fiber optic placed at the prime focus of the telescope illuminates a screen with the patterns shown in the lower two rows of figures. The first and last images show no indication of a pattern since these positions were outside of the telescope aperture.

or secondary telescope, either not sampled by the lamp or undersampled by the lamp, changes over time, then the results of the lamp calibration will not accurately reflect these changes. Also, if some debris were to fall on the telescope just at the point where the forward beam is making its intense spot, a change in the efficiency ratio would likely be quantified where such a change would not represent the majority of the telescope aperture.

The possibility of position-dependent changes in the optical efficiency of components of the optical train are not limited to the primary or secondary mirrors. For example, photomultiplier tubes [10] and interference filters, commonly used in lidar receiver optical configurations, are known to be capable of position-dependent efficiency changes. An example of the position dependence of the transmission efficiency and bandpass of a narrow-band interference filter is given in Fig. 3. The transmission of the 2 in. diameter filter was determined with a beam approximately 0.5 in. in diameter. The transmission was quantified with the beam centered on the filter and offset approximately 0.5 in. from the center. The transmission is observed to increase significantly at this offset position. A technique that fully samples the telescope aperture can be used to circumvent the position-dependent concerns described here. The next Section illustrates such a technique.

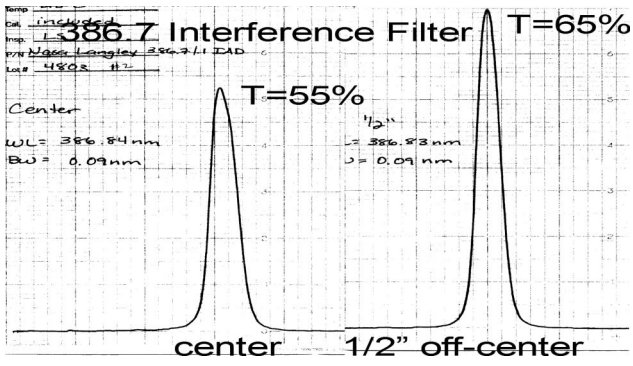

Fig. 3. Bandpass of a 0.1 nm interference filter used to measure Raman scattering from atmospheric nitrogen. The transmission of the central 1/2 in. of the filter is approximately 55% while 1/2 in. off-center the transmission increases to 65%.

5. Scanning the Full Aperture of the Lidar Receiver

A tungsten calibration lamp offers a highly stable ratio of output intensities at the water vapor and nitrogen wavelengths. The problems illustrated above come about by undersampling the telescope aperture using such a lamp. A technique involving movable *X*–*Y* stages that can permit the lamp to scan the full aperture of a receiver telescope has been under development since 2006 as a joint project involving Howard University, Instituto de Pesquisas Energéticas e Nucleares (IPEN) in Brazil and National Aeronautics and Space Administration/

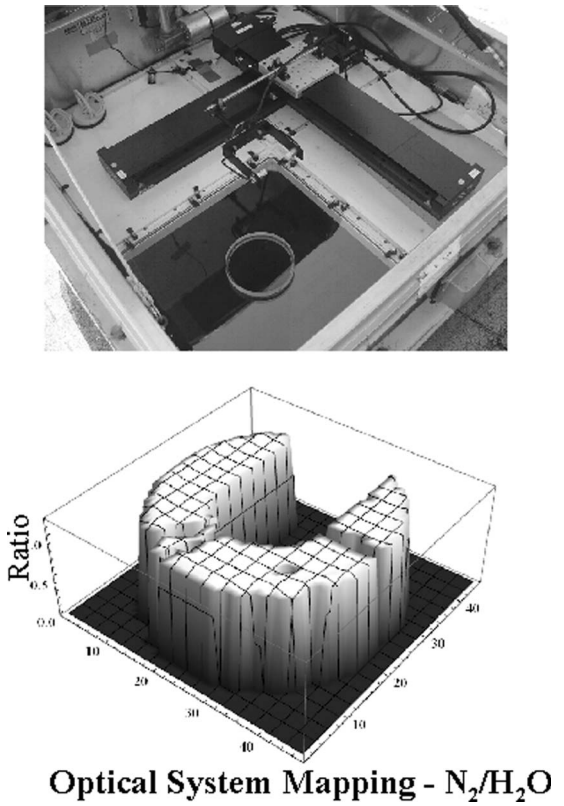

Fig. 4. System for translating a calibration lamp across the full aperture of a lidar receiver telescope is shown in the upper photo. A map of the ratio of total optical system efficiencies as a function of the position across the telescope input aperture obtained with the translating calibration lamp is shown in the bottom of the figure. Dropouts due to a horizontal periscope, secondary spider veins, and other obstructions are apparent in the mapping.

Goddard Space Flight Center (NASA/GSFC) [11–13]. The calibration lamp is moved in small, even increments across the full useful aperture of the receiving telescope. At each location, the signals in the water vapor and nitrogen channels are quantified by the lidar data acquisition system using equal sampling time at each location. The ratio of the water vapor and nitrogen signals are then determined as a function of the position. The efficiency ratio that characterizes the full optical system is then taken to be the average of all of the individual ratios after excluding data subject to edge effects (where not all of the lamp is directly illuminating the telescope primary). A photograph of the ganged X–Y stages in position above the HURL transmission window and an example of the scanned data obtained is shown in Fig. 4. The scanning experiment provides measurements at approximately 300 different locations on the telescope. These measurements are filtered to eliminate edge effects or areas with known obstructions. A histogram of the remaining 193 individual cells that constitute a full-aperture scan is shown in Fig. 5. The mean value of the individual cells is 1.157 ± 0.013. The range of efficiency ratios is 1.116 to 1.190 indicating approximately a 7% variation in the measured efficiency ratio over the useful aperture of the telescope.

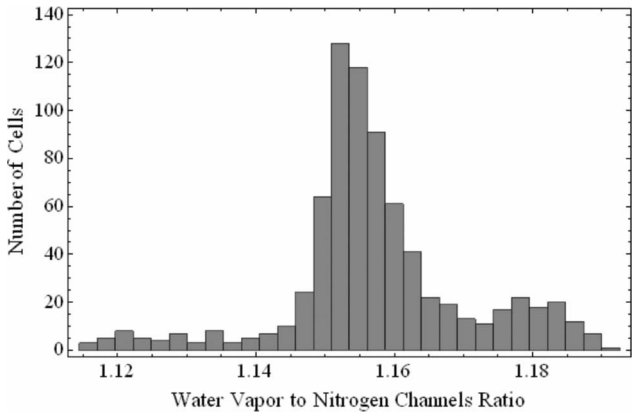

Fig. 5. Histogram of the measured efficiency ratios recorded using a calibration lamp scanned over the full aperture of the HURL. The range of measured values is approximately 7%.

6. Failure Modes of a Calibration Lamp

Even though scanning the full lidar telescope aperture with a calibration lamp provides an improved characterization of the full lidar receiver optical efficiency when compared with using a lamp in a fixed position, there are still "failure modes" that both techniques share in common that will now be described. Consider that the Raman return signals for water vapor and nitrogen excited in the atmosphere by a narrowband laser have a small spectral width on the order of 0.1–0.2 nm. Interference filters in use in Raman water vapor lidar measurements range from 0.1–1.0 nm typically and exhibit significant transmission variation over their nominal bandpass. These filters are angle sensitive so that small changes in the tilt angle of the filter can result in significant changes to the transmission efficiency of the desired Raman signal. However, the output of a calibration lamp is nearly uniform for the same small changes in wavelength. This implies that if a filter angular displacement were to occur, the lamp technique would not properly account for the change in effective efficiency ratio. A similar statement could be made with respect to the slit position if a grating spectrometer is used to select the passband.

To illustrate this, an experiment was performed using the NASA/GSFC ALVICE lidar system. [14] Daytime measurements of water vapor mixing ratios were made on 24 April, 2009 using two minute summations at various tilt angles ranging from 2–6° for a 0.1 nm Raman N_2 filter. (The peak transmission for the filter in use was obtained at a filter tilt angle of approximately 1–2°.) A tilt of 1° changes the center wavelength position of the filter by approximately 0.02 nm, or about 20% of the bandwidth, so a significant change in transmission efficiency of the filter is expected. For this exercise, the mixing ratio values above the boundary layer were assumed constant over the approximate 1 h that was required to perform the experiment. A different normalization value was used for each profile to achieve best agreement among all the profiles above the boundary layer. The

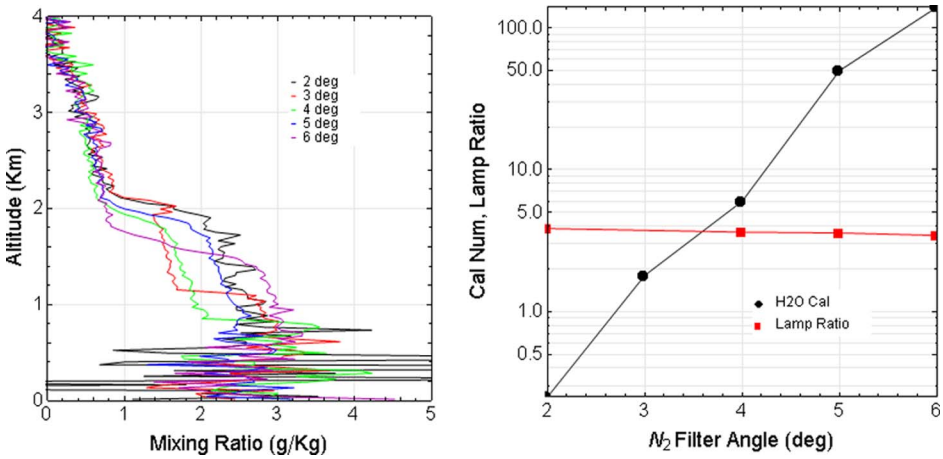

Fig. 6. (Color online) (Left) A series of water vapor mixing ratio profiles taken with the N_2 filter at various tilt angles. The profiles have been individually calibrated. Efficiency ratios using a calibration lamp were quantified at each angle. (Right) The calibration number required for each of the profiles shown on the left along with the measured lamp ratios at each angle. No lamp data were acquired when the filter was tilted at an angle of 3°.

normalization values used are plotted in Fig. 6 and range from 0.25 to 140, indicating that the nitrogen filter transmission changes by more than 2 orders of magnitude over this set of tilt angles. At the same time, the efficiency ratio recorded at each angle setting using the calibration lamp changes by less than 10%. The lamp calibration is not useful to detect changes in the center wavelength of the filter, which could be caused in the short term by a mechanical disturbance of the filter or in the long term by a filter degradation.

Another failure mode of either lamp calibration technique is also a failure mode of all the dominant calibration techniques, when measurements extending into the dry upper troposphere are considered. The calibration approaches of simple radiosonde matching in the lower to middle troposphere [6], radiosonde + calibration lamp [6], total column water scaling [15], calibration assuming saturation at cloud base [16], or absolute calibration efforts [12,17] will not detect errors in Raman water vapor lidar mixing ratio measurements in the upper troposphere due to such effects as signal-induced noise or fluorescence [1,18]. To guard against errors created by effects such as these, comparison of the final lidar profile of water vapor with another instrument, such as cryogenic frostpoint hygrometer or well-validated satellite measurements, such as the Aura Microwave Limb Sounder [19], will likely need to be done on a periodic basis.

7. Discussion and Conclusion

A tungsten calibration lamp provides a very stable ratio of outputs at the Raman water vapor and nitrogen wavelengths used for Raman water vapor lidar measurements of water vapor mixing ratio. Such a lamp has been found useful for quantifying the efficiency ratio at these two wavelengths as a method for improving on the technique of calibrating Raman water vapor lidar with respect to radiosondes [6]. This technique uses one calibration lamp at a time in a fixed position in front of the telescope aperture. As discussed in [6], this technique can be useful in combination with radiosonde data to distinguish variations in calculated calibration coefficients that may be due to atmospheric variation instead of lidar system efficiency variation. The use of lamps to aid Raman water vapor lidar calibration is therefore currently being encouraged within the NDACC. We have focused here on issues that can be presented by using a single, fixed lamp as a tool for quantifying the ratio of optical efficiencies of the lidar channels. The uneven sampling of the lidar optical system aperture makes the technique susceptible to certain errors that do not plague traditional calibration approaches. If, for example, a small piece of debris were to fall onto the telescope at just the location where the calibration lamp makes its intense spot in the forward direction onto the primary mirror, a spurious calibration result could be obtained. Because of this, changes in calibration that are indicated by this technique would need to be further investigated as to their source instead of assuming that they necessarily are due to an overall lidar system optical efficiency change.

As a simpler alternative to scanning the full aperture of the telescope, an experimental configuration involving multiple calibration lamps used in different fixed positions in front of the telescope would provide some redundancy to help detect anomalous efficiency ratio measurements. Each of the lamps could be run sequentially as a part of each "lamp calibration" exercise. The intensity ratios recorded by the all the lamps could then be monitored. A change in the efficiency ratio recorded from the output of just one lamp would indicate a spurious, localized effect. Whereas, an intensity ratio change recorded from the output of all lamps would indicate the need for a different lidar calibration constant. How many lamps would be sufficient to serve as a satisfactory replacement for fully scanning the telescope aperture should be a subject of future experimentation, but the full-aperture scanning experiments shown here and also being performed at IPEN [12] can be used

to shed light on this question. The discussions contained here also indicate that reflections from uncalibrated surfaces should be avoided in the application of lamp-based calibration techniques.

The influence of changes in the center wavelength of the bandpass filters, such as could result if the receiver optics were mechanically disturbed, cannot be detected using lamp-based techniques. To ensure that no such disturbance has occurred, it will be necessary to periodically check that the transmission peaks of the filters or spectrometer in use are properly aligned with the Raman spectral features. This can be done experimentally by tilting the interference filters and recording the signals as was done to create Fig. 6. Careful application of this technique can ensure that the filters are centered, for example on the point of maximum signal strength which is a repeatable configuration. The temperature sensitivity of Raman scattering for both N_2 and H_2O, which can influence the calibration of Raman water vapor lidar systems [20,21], can then be calculated using these known spectral locations.

Finally, there is a failure mode that is shared by both lamp-based calibration techniques and more traditional ones as well when considering measurements of upper tropospheric or lower stratospheric water vapor. Small amounts of signal-induced noise or fluorescence can contaminate these high altitude measurements in a manner that could be detected only through a direct comparison with an external source believed to be accurate at these high altitudes. Such comparisons, whether with balloonborne sensors, such as cryogenic frostpoint hygrometer or well-validated satellites, such as microwave limb sounder, will be needed periodically to gauge the performance of Raman lidar at high altitudes.

The authors wish to acknowledge the NASA Atmospheric Composition Program for support of these efforts.

References

1. T. Leblanc, I. S. McDermid, and R. A. Aspey, "First-year operation of a new water vapor Raman lidar at the JPL Table Mountain Facility, California," J. Atmos. Ocean. Technol. **25**, 1454–1462 (2008).
2. D. J. Seidel, F. H. Berger, H. J. Diamond, J. Dykema, D. Goodrich, F. Immler, W. Murray, T. Peterson, D. Siststerson, M. Sommer, P. Thorne, H. Vömel, and J. Wang, "Reference upper-air observations for climate: rationale, progress, and plans," Bull. Am. Meteorol. Soc. **90**, 361–369 (2009).
3. E. C. Weatherhead, G. C. Tiao, G. C. Reinsel, J. E. Frederick, J. J. DeLuisi, D. Choi, and W.-K. Tam, "Analysis of long-term behavior of ultraviolet radiation measured by Robertson-Berger meters at 14 sites in the United States," J. Geophys Res. **102**, 8737–8754 (1997).
4. E. C. Weatherhead, G. C. Reinsel, G. C. Tiao, X.-L. Meng, D. Hoi, W.-K. Cheang, T. Keller, J. DeLuisi, D. J. Wuebbles, J. B. Kerr, A. J. Miller, S. J. Oltmans, and J. E. Frederick, "Factors affecting the detection of trends: statistical considerations and applications to environmental data," J. Geophys. Res. **103**, 17,149–17,161 (1998).
5. R. Boers and E. Meijgaard, What are the demands on an observational program to detect trends in upper tropospheric water vapor anticipated in the 21st century, Geophys. Res. Lett. **36**, L19806 (2009).
6. T. Leblanc and I. S. McDermid, "Accuracy of Raman lidar water vapor calibration and its applicability to long-term measurements," Appl. Opt., **47**, 5592–5603 (2008).
7. D. N Whiteman, "Examination of the traditional Raman lidar technique. I. Evaluating the temperature-dependent lidar equations," Appl. Opt. **42**, 2571–2592 (2003).
8. D. N. Whiteman, "Examination of the traditional Raman lidar technique. II. Evaluating the ratios for water vapor and aerosols," Appl. Opt. **42**, 2593–2608 (2003).
9. Optronics Laboratories, 4632 36th Street Orlando, FL 32811 (personal communication, 2009).
10. V. Simeonov, G. Larcheveque, P. Quaglia, H. van den Bergh, B. Calpini, "Influence of the photomultiplier tube spatial uniformity on lidar signals," Appl. Opt. **38**, 5186–5190 (1999).
11. A. S. Torres, E. Landulfo, D. N. Whiteman, and D. Venable, "Water vapor raman lidar independent calibration," presented at the 24th International Laser Radar Conference, Boulder, Colorado, USA, 23–28 June 2008.
12. E. Landulfo, R. F. Da Costa, A. S. Torres, F. J. S. Lopes, D. N. Whiteman, D. D. Venable, "Raman water vapor lidar calibration," Proc. SPIE **7479**, 74790J (2009).
13. D. D. Venable, D. N. Whiteman, M. N. Calhoun, A. O. Dirisu, R. N. Connell, and E. Landulfo are preparing a manuscript to be called "A lamp mapping technique for independent determination of the water vapor mixing ratio calibration factor for a Raman lidar system."
14. D. N. Whiteman, K. Rush, S. Rabenhorst, W. Welch, M. Cadirola, G. McIntire, F. Russo, M. Adam, D. Venable, R. Connell, I. Veselovskii, R. Forno, B. Mielke, B. Stein, T. Leblanc, S. McDermid, and H. Vömel, "Airborne and ground-based measurements using a high-performance Raman lidar," J. Atmos. Ocean. Technol. **27**, 1781–1801 (2010).
15. D. D. Turner, R. A. Ferrare, L. A. H. Brasseur, W. F. Feltz, "Automated retrievals of water vapor and aerosol profiles from an operational Raman lidar," J. Atmos. Ocean. Technol. **19**, 37–50 (2002).
16. D. N. Whiteman, K. D. Evans, B. Demoz, D. O'C. Starr, E. Eloranta, D. Tobin, W. Feltz, G. J. Jedlovec, S. I. Gutman, G. K. Schwemmer, M. Cadirola, S. H. Melfi, and F. J. Schmidlin, "Raman lidar measurements of water vapor and cirrus clouds during the passage of hurricane Bonnie," J. Geophys. Res. **106**, 5211–5225 (2001).
17. V. Sherlock, A. Hauchecorne, J. Lenoble, "Methodology for the independent calibration of Raman backscatter water-vapor lidar systems," Appl. Opt. **38**, 5816–5837 (1999).
18. V. Sherlock, A. Garnier, A. Hauchecorne, and P. Keckhut, "Implementation and validation of a Raman lidar measurement of middle and upper tropospheric water vapor," Appl. Opt. **38**, 5838–5858 (1999).
19. H. Vömel, J. E. Barnes, R. N. Forno, M. Fujiwara, F. Hasebe, S. Iwasaki, "Validation of aura microwave limb sounder water vapor by balloonborne cryogenic frost point hygrometer measurements," J. Geophys. Res. D **112**, D24S37 (2007).
20. D. N. Whiteman, B. Demoz, P. Di Girolamo, J. Comer, I. Veselovskii, K. Evans, Z. Wang, D. Sabatino, G. Schwemmer, B. Gentry, R.-F. Lin, A. Behrendt, V. Wulfmeyer, E. Browell, R. Ferrare, and S. Ismail, J. Wang, "Raman water vapor lidar measurements during the International H2O Project. II. Case studies," J. Atmos. Oceanic Technol. **23**, 170–183 (2006).
21. D. N. Whiteman, F. Russo, L. Miloshevich, B. Demoz, Z. Wang, I. Veselovskii, H. Voemel, S. Hannon, B. Lesht, F. Schmidlin, A. Gambacorta, and C. Barnet, "Analysis of Raman lidar and radiosonde measurements from the AWEX-G field campaign and its relation to Aqua validation," J. Geophys. Res. **111**, D09S09 (2006).